A Simple Approach to Predictive Control for Small Wind Turbines with an Application to Stress Alleviation

Marco Garcia, Juan C. San-Martin, Antonio Favela-Contreras, Luis I. Minchala, Diego Cardenas-Fuentes, Oliver Probst

Tecnologico de Monterrey, Ave. Eugenio Garza Sada 2501, CP 64849, Monterrey, NL, Mexico (e-mail: oprobst@itesm.mx)

Abstract: Small wind turbines (SWT) generally operate under unsupervised conditions, often exposed to varying environmental conditions including high turbulence and gust levels. While traditional SWT control focuses on maximum power point tracking (MPPT), a reliability-oriented design should also consider an appropriate strategy for mitigating mechanical loads in the rotor and other structural elements. In the present work, a predictive control-based strategy is presented which allows to upgrade an existing small wind system by implementing a supervisory control considering a joint optimization of output power and the stress in the rotor blades. Innovations include a simple yet robust implementation of an adaptive predictive control for a custom-designed rectifier and the construction of a compound objective function through advanced beam modelling of the rotor blades. The proposed strategy has been demonstrated experimentally using a laboratory test bench, showing a significant reduction of rotor stress while maintaining the SWT near optimal power extraction conditions.

Keywords: APC, blades, control, load reduction, small wind turbine.

1. INTRODUCTION

The growth of large-scale wind energy has reached promising levels worldwide. The global installed capacity re- ported in 2014 was 370 GW (Gupta and McIntyre, 2017), and it is expected to reach 1013 GW by 2025 (Frost and Sullivan, 2017). The continued evolution of government regulations and standards and their implications for fossil fuel replacements are considered one important driver for wind energy growth. It is expected that the Paris Agreement (UNFCCC, 2015) signed by 165 countries will pro- vide additional momentum to the transition towards clean energies. However, despite the encouraging development of large-scale wind power plants, the utilization of wind energy in small wind turbines (SWT) and systems is progressing much more slowly, with barriers including a higher cost on a kW-basis and the need to guarantee reliable operations under essentially unsupervised conditions and minimal maintenance over extended periods of time.

Decreasing the total life cycle cost (TLC) of wind energy conversion systems (WECS) is currently one of the main tasks of industry and researchers to foster the adoption of these systems. A feasible solution is to increase the rotor size for the same drive train and rated power, which produces a higher energy harvested by the rotor for a given rated generator capacity. The main drawback of this alternative is the significantly increase of the fatigue and extreme loads of the wind turbine (WT). To address this issue, (Iordanov et al., 2017) propose providing wind turbines with more intelligence by developing a self-operation multi-objective control strategy. To this end, all the instrumentation installed in the WT is used to monitor/estimate physical variables, and to support the development of other applications, *e.g.* advanced control algorithms to reduce structural loads (Petrović et al., 2015) and advanced monitoring of blade conditions (Yang et al., 2014), *etc*.

Rotor rotation causes structural vibrations over the blades, which potentially increment fatigue and reduce the expected life of the wind turbine (Mishnaevsky et al., 2012). The reasons for these oscillations include gravity, wind shear, yaw misalignment, tower shadow, and the stochastic nature of the wind field (Wymore et al., 2015). Wind turbines of great sizes handle these issues typically through pitch control techniques, such as cyclic pitch control (Bottasso et al., 2014), collective pitch control (Han and Liu, 2014; Meng et al., 2016), and individual pitch control (Selvam et al., 2009; Han and Leithead, 2014). Small wind turbines (SWT), however, are often designed to work with a fixed pitch angle; therefore, the alleviation of dynamic and structural loads has to be handled by other approaches. For instance, (González et al., 2010) present a method to obtain a soft dynamic response of torque and speed of a SWT by using a sensorless MPPT algorithm, which offers a reduced mechanical stress compared with conventional perturb & observe techniques. (Senanayaka et al., 2017) propose a soft-stall power control based on a sliding-mode algorithm to reduce unbalanced forces on the blades. The simulation results show an enhanced energy harvest of 13% compared to other stalling techniques.

The majority of control strategies for SWT focus on MPPT techniques, leaving other variables unattended, such as structural loads. For instance, (Habibi et al., 2017) propose a fuzzy control approach for adjusting the generator torque in the partial load regime of a WT. The main purpose of the control strategy is to track the ideal power curve without incrementing the stress of the

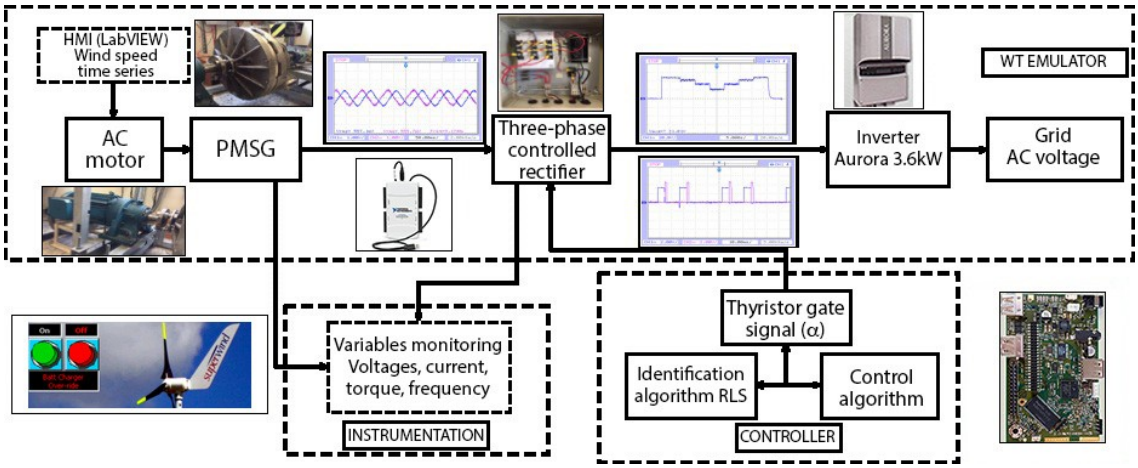

Fig. 1. Test bench setup.

main shaft of the WT. Traditionally, the rotor speed regulation of an SWT is used to maximize the power extraction from the wind. It should be noted that, it is also possible to use speed regulation in an SWT to minimize the loads on its structure, the shaft, and the blades. For instance, the blades absorb peaks of the torque during the variation of the speed of rotation of the generator, leading to a longer installation life of the WECS (Ghosh et al., 2014). (Scarlat et al., 2012) present an active speed stall technique for power limitation in Region III of operation of a WT, as well as the power maximization in Region II of a WT by acting on the rotational speed through the variable-speed control infrastructure. The proposed control structure is implemented by means of output power control loop that ensures WECS operation over the entire wind speed variation range. Experimental results on a test rig demonstrate the effectiveness of the proposed controller. (Minchala et al., 2018) show a simulation-based approach of a non-linear model predictive control (NMPC) applied to a WT. The NMPC works as a supervisory controller, which optimizes a predefined relationship between the power captured from the wind and the stress over the blades of a WT by calculating the setpoints of distributed controllers of a classic control architecture of WTs.

This work proposes a simple, yet robust implementation of an adaptive predictive control (APC) for a custom-designed rectifier to regulate the rotor speed and avoid the adverse effect of extreme loads and fatigue damages over the blades of a variable speed SWT. The proposed control strategy optimizes a compound objective function developed through advanced beam modeling of the rotor blades to balance the mechanical stress and the power harvested from the wind. This controller has a two-level architecture, as follows:

- Supervisory level. This level consists of an optimal regulator, which performs a joint optimization of a compound objective function that relates the power output and the stress over the blades.
- Distributed control. This layer implements an adaptive predictive controller to regulate the output voltage of a three-phase controlled rectifier. The controller's set-point is received from the supervisory level. The voltage regulation on the rectifier allows the adjustment of the rotor speed in the WT.

This paper is organized as follows: Section II presents the architecture of the laboratory test bench. Section III describes the design of the control strategy. In section IV the experimental results obtained with an instrumented laboratory test rig are shown and discussed. The main lessons learned are described in section V.

2. WIND TURBINE EMULATOR

The laboratory test bench used for this research emulates the down-scaled version of a 10kW variable speed wind turbine, rated at 3kW. The test bench was developed through the combination of dedicated hardware and software. Fig. 1 shows the general architecture of the laboratory setup.

Among the main features of the system, the following should be mentioned:

- Variable wind speed emulation according to a stochastic time series.
- Measurement of process variables: mechanical torque (T_m), three-phase currents and voltages (i_{abc}, v_{abc}), generated power (P), frequency (f), rotor speed (ω_r). Realistic configuration through the use of commercial hardware components, including a 3.6kW Aurora inverter.
- Possibility of emulation of wind turbines with different characteristics by updating C_p (λ).

The home-built permanent magnet synchronous generator (PMSG) is coupled with a prime mover, which consists of a variable speed three-phase induction motor. Fig. 2 shows the algorithm used to adjust the speed velocity of the PMSG according to a wind speed time series, and the emulated wind turbine characteristics. The C_p (λ) curve was calculated using blade element momentum (BEM) theory. BEM models are generally found to yield accurate predictions of the

field behavior of wind turbines; see *e.g. (*Elizondo et al., 2009).

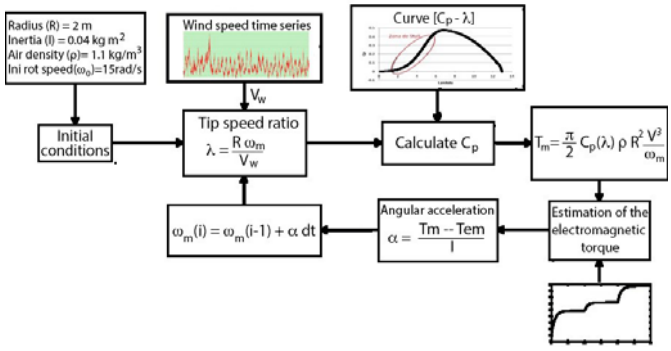

Fig. 2. Control algorithm for variable wind speed emulation in the laboratory test bench.

3. ADAPTIVE PREDICTIVE CONTROL

The APC control algorithm allows real-time identification of the parameters of a dynamical model structure of a system in order to calculate efficient control actions. The most commonly used identification method is the recursive least square (RLS) algorithm (Bobrow and Murray, 1993), which provides a discrete-time representation of an autoregressive model with exogenous input (ARX).

In this research, the APC implementation was carried out by using the well-known general predictive control (GPC) proposed by D.W. Clarke (Clarke et al., 1987). In adaptive control applications, it is common practice to select GPC due to its robustness. The GCP minimizes a multi-stage cost function over a given prediction horizon (Chidrawar and Patre, 2008).

3.1 General predictive control

The GPC operation initiates with the application of an input signal $r(t)$ to a reference model to generate a tracking input $w(t)$ to be applied to the minimization algorithm of the cost function, J. The result of the optimization is the control signal $u(t)$. The cost function uses the dynamic model of the system to calculate $u(t)$ through the solution of an optimal control problem, which is composed of the cost function and operational constraints.

Fig. 3. shows a general block diagram of the GPC structure. The mathematical formulation of the GPC is as follows:

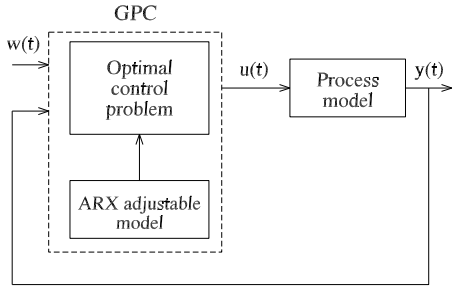

Fig. 3. Basic structure of the GPC algorithm.

$$A(z^{-1})y(t) = z^{-d}B(z^{-1})u(t-1) + C(z^{-1})\frac{e(t)}{\Delta} \quad (1)$$

where $A(z^{-1})$ and $B(z^{-1})$ are the discrete polynomials of the system transfer function numerator and denominator, respectively; $C(z^{-1})$represents a moving average error calculation; d represents the system time delay; *e(t)* represents white noise with zero mean signal; *u(t)* represents the control signal.

The minimization algorithm of the cost function is based on Eq. (2), where the optimal trajectory of $y(t + j)$ for $N_1 \leq j \leq N_2$ is computed by minimizing:

$$J(N_1, N_2, N_u) = \sum_{j=N_1}^{N_2} \delta(j)[\hat{y}(t+j|t) - w(t+j)]^2 + \sum_{j=1}^{N_u} \lambda(j)[\Delta u(t+j-1)]^2 \quad (2)$$

where,

N_1, N_2, N_u	Prediction and control horizon limits
$\delta(j)$, $\lambda(j)$	Weighting factors
$w(t+j)$	Trajectory of reference
$\hat{y}(t+k-i)$	Output predictor
$\Delta u(t+k-i)$	Control signal deviation
$J(N_1, N_2, N_u)$	Cost function

In addition, the diophantine equation, Eq. (3), must be satisfied:

$$1 = E_j(z^{-1})\Delta A(z^{-1}) + z^{-j}F_j(z^{-1}) \quad (3)$$

where E_j, F_j are polynomials of order $j-1$ and *na*, respectively, obtained from the recursive division of 1 and $\tilde{A}(z^{-1}) = \Delta A(z)$, until the residue can be factored as $z^{-j}F_j(z^{-1})$ and the quotient is the polynomial $E_j(z^{-1})$.

The GPC preserves the inherent advantages of the adaptive control in stochastic systems, allows online identification of the system model, and allows the planning of a control strategy within a moving horizon in a similar manner of the efficient model predictive control. Additionally, precision requirements in the model are not strict.

3.2. APC control design

Fig. 4 shows the set of power curves $P(n, v)$ of the WT under study, where n is the rotor speed in rpm and v the wind speed in m/s. The wind speed and the rotor velocity determine the power which can be extracted by the rotor. The maximum power which can be extracted at a given wind speed is given by the red line in Fig. 4; its points are known as the maximum power points (MPP). Most wind turbine control strategies focus on attaining and maintaining MPP conditions and are therefore known as MPP tracking (MPPT) strategies. In the present work, a more general approach will be presented where through the use of an objective function containing information about both the rotor

power and mechanical stresses at critical blade locations – a bi-objective control can be realized.

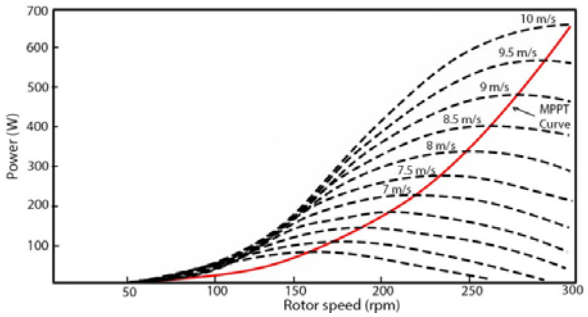

Fig. 4. Power curve of the wind turbine under study.

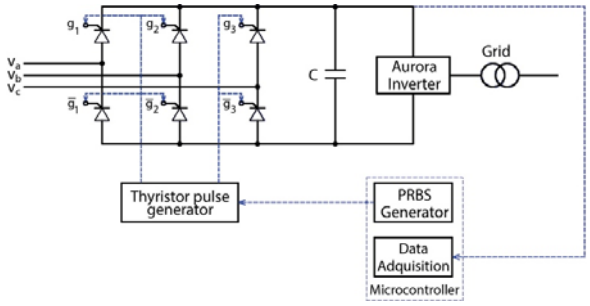

Fig. 5. System identification setup for the WECS.

The APC design, based on the GCP algorithm, consists in identifying the dynamic model of the WECS. The control variable is the firing angle of the gate signals of the thyristors of a three-phase rectifier $[g_1, \overline{g}_1, g_2, \overline{g}_2, g_3, \overline{g}_3]$. The system identification by using the RLS methodology starts with the calculation of a static model by using the least squares algorithm and a data set. Fig. 5 shows the architecture of the corresponding system identification setup. The identification signal used for the estimation of the static model is a pseudo-random binary signal (PRBS).

Fig. 6 shows four different response voltage curves obtained from the identification process, by applying the PRBS signal to the gate activation signals of the thyristors. Every curve has a different mean rotor speed value ($\overline{\omega}_r$). Different percentages of adjustment of the ARX models to the identification data set are obtained in each test. Table 1 shows a summary of the ARX models obtained with these identification tests.

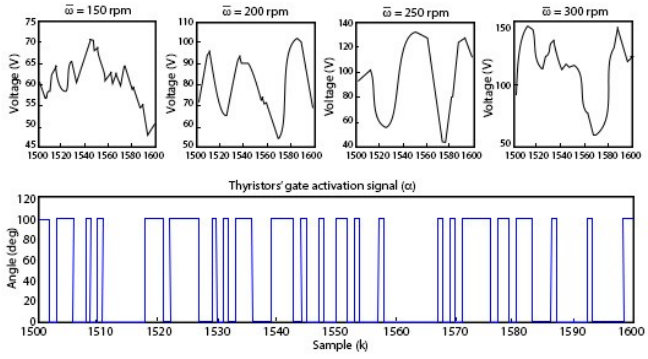

Fig. 6. Response curves of the identification process for the WECS.

The model with the best data fit is the one corresponding to $\overline{\omega} = 300rpm$ with the following structure:

Table 1. Results summary of the identification process of the WECS.

□r (rpm)	Coefficients of the ARX model			Data fit (%)
	a_0	b_1	b_2	
150	0.967534	0.000769	0.010427	84.6
200	0.975912	0.004829	0.015027	92.2
250	0.986393	0.007560	0.018198	94.2
300	0.987795	0.008188	0.021897	95.1

$$G_p(z) = \frac{b_1 + b_2 z^{-1}}{1 - a_0 z^{-1}} = \frac{0.04828 + 0.01502 z^{-1}}{1 - 0.9759 z^{-1}} \quad (4)$$

Additionally, to complete the APC design it is necessary to define an optimization/prediction horizon (N1, N2, Nu), as well as a conducting block transfer function (desired trajectory generator). The desired trajectory of this design corresponds to a first order fast-response system, with the following structure:

$$G_d(z) = \frac{0.9932}{1 - 0.06737 z^{-1}} \quad (5)$$

Fig. 7 shows a block diagram of the APC control system with the following elements:

- Conductor block: Eq. (5)
- Predictive control: Equations (2)-(3)
- Adaptive mechanism: RLS algorithm for updating the initial ARX model
- Model of the process: Eq. (4)
- Reference: *argmin* {Eq. (6)}

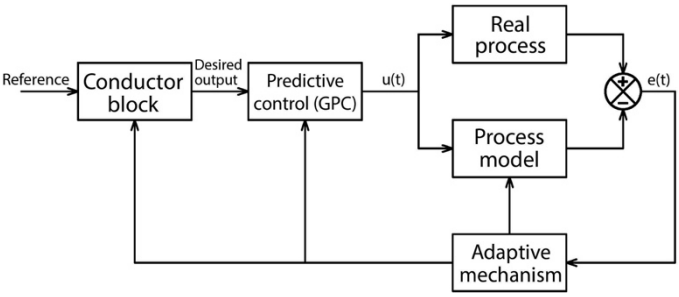

Fig. 7. APC block diagram.

3.3 Integration of the APC algorithm with the supervisory control scheme

The supervisory control scheme to be used in this implementation, calculates the set-point of the rotor speed control loop (ω_{ref}), which depends on the variable output voltage of the three-phase rectifier. The regulation of the output voltage of the rectifier is performed by the APC.

The cost function of the supervisory scheme is the following:

$$f(\omega, V_w) = P(\omega_r, V_w) - \kappa\xi(\omega_r, V_w) \quad (6)$$

where,

P	Normalized output power curve
ω_r	Rotor speed
ξ	Normalized instantaneous stress over the blades
κ	Penalty variable of ξ (design variable)
V_w	Wind speed

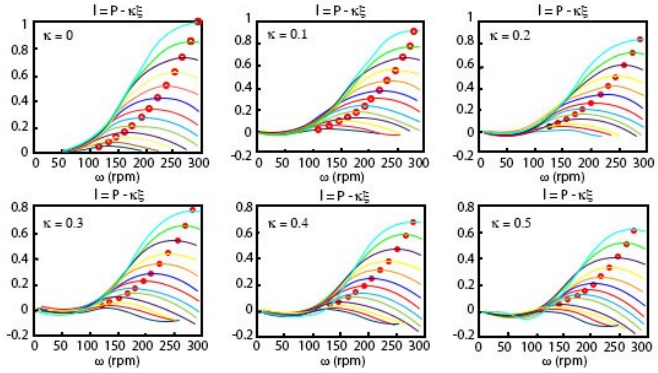

Fig. 8. Graphical response of the bi-objective function, Eq. (6), for different values of κ.

The normalized instantaneous stress at the critical location of the blades is calculated by using an integrated BEM/TWM model presented in (Minchala et al., 2017); an application to fatigue damage propagation in wind turbine blades described in Cárdenas et al. (2018). ξ depends on the rotor speed in rpm and the wind speed in m/s.

Graphical responses of the cost function (6) for swept values of ω_r, and different values of κ are shown in Fig. 8. In the present work, a constant blade pitch angle of 0 is assumed at all times, given the fixed-pitch design of the small wind turbine under study. The approach presented can however be generalized to the case of a variable pitch angle. Values of $\kappa > 0.5$ produces negative values in the cost function, which is not permitted. Therefore, an optimization constraint is $\kappa < 0.5$. A reliable operation of the wind turbine must guarantee $\xi < 1$.

The ω_{ref} value depends on the optimal value of the rectifier output voltage, v_{dc}^*, which is obtained off-line through a linear search of the maximum power tracking and the minimum stress factor over the blades, argmin {Eq. (6)}. Several off-line linear searches for different operating conditions of the wind turbine are performed by using a linear programming (LP) algorithm, which allowed the calculation of an approximate optimal solution through a polynomial expression, in the form:

$$v_{dc}^* = \alpha_1 V_w^3 + \alpha_2 V_w^2 + \alpha_3 V_w + \gamma \quad (7)$$

where v_{dc}^* is the reference signal for the APC algorithm; V_w is the wind speed; α_1, α_2, α_3, and γ are obtained by data fitting the optimization results calculated off-line. The solution of this bi-objective cost function allows for a simple, yet powerful, two-layer control strategy. The upper layer calculates the optimal voltage output of the three-phase rectifier by solving Eq. (7). The lower layer implements the APC algorithm by using the previously calculated reference, which is directly related with the rotor speed reference, (ω_{ref}).

The penalty variable κ produces different responses in the optimization result. Fig. 9 shows the variation of the optimal value of the cost function in the power-stress plane for different values of κ, and different wind speed values. It is important to notice that the impact of the penalty factor κ on the normalized power is relatively small, compared to the substantial reductions in normalized stress obtained in return, as illustrated by the nearly horizontal curves.

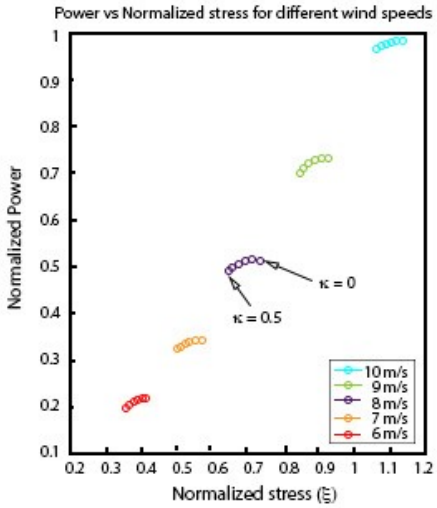

Fig. 9. Relationship between the power offer and the stress over the blades for different values of κ and V_w.

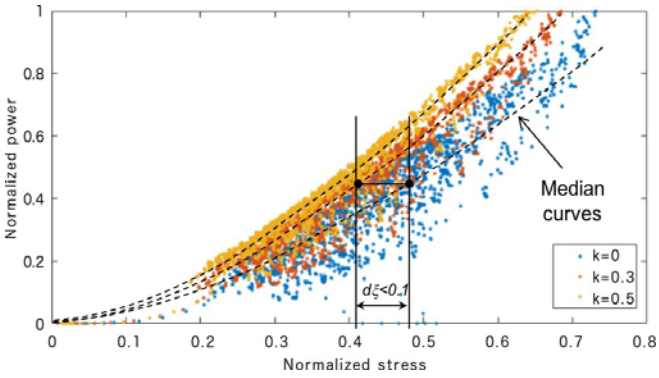

Fig. 10. Scatter plot of experimental data for normalized stress and normalized power for different values of κ.

4. EXPERIMENTAL RESULTS

In order to demonstrate the advantages of the proposed control system, an experimental setup using the laboratory test bench described above was established. To assess the efficacy of the proposed APC scheme, a baseline controller based on a PID approach was also implemented and tested alongside with the APC control. Both, the PID and the APC controllers were deployed in an embedded microcontroller platform to provide a real-time implementation.

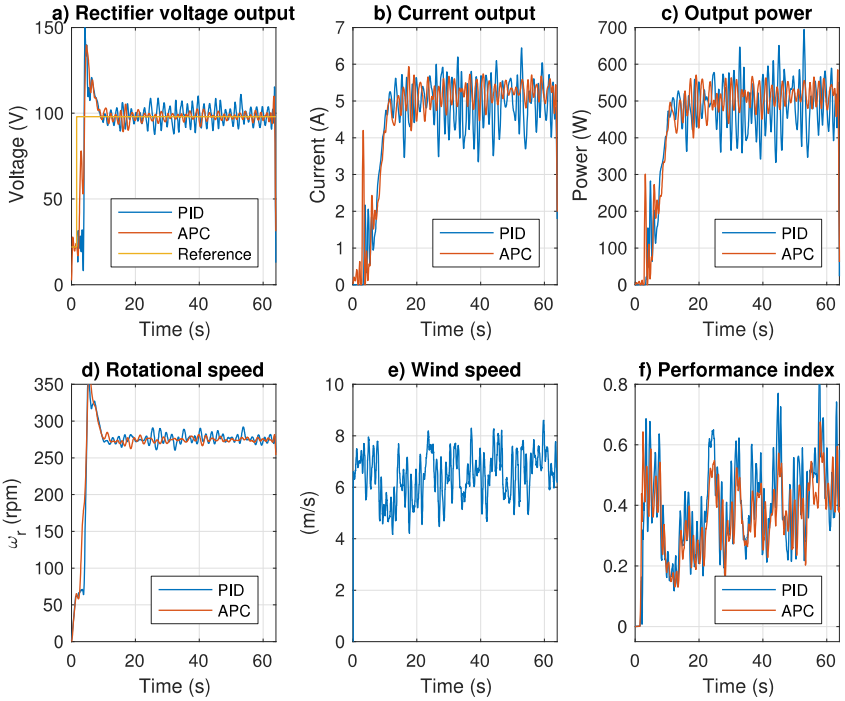

Fig. 11. Comparison of the performance of the proposed APC vs the reference PID strategy.

It will first be shown how the use of the compound cost function of Eq. (6) instead of the usual power function impacts on the power-stress trajectories experienced by the emulated wind turbine. Fig. 10 shows scatter plots of ξ and the normalized power obtained from experimental results of the test rig when operating with the proposed APC controller tuned to different values of κ. The wind speed time series used for this test has low turbulence intensity, and a mean wind speed of 6 m/s. The dots pertaining to $\kappa = 0$ correspond to a conventional MPPT strategy without stress control. It can be seen from Fig. 10 that for a given power level a significant reduction in stress is achieved; conversely, for a given tolerable stress level the output power is considerably higher with the new method proposed, compared to the traditional MPPT approach. For the example shown in Fig. 10 a median reduction of about 0.1 p.u. in stress is obtained at a power level of 0.4 p.u. when setting the penalty factor κ to 0.3, instead of using the MPPT-value of $\kappa = 0$. The median curves drawn over the dots of the operation of the system for different values of κ demonstrate the consistency of the experimental results with the theoretical expectations based on the evolution of the set points in the power-stress plane (Fig. 9) in response to a change in the penalty factor κ. The selection of κ corresponds to the controller's tuning, and the best practical result was obtained with $\kappa = 0.3$. In the results presented below κ was kept at 0.3 at all times.

Fig. 11 shows the comparison of the performance between the APC and PID controllers for a wind speed time series with the characteristics described above. The first 10 seconds of the system response correspond to a transient behavior due to a step change in the voltage reference. The overshoot in both controllers is about 40%, and the settling time is 15 seconds. The output voltage of the three-phase rectifier is kept around 98 V, which leads to a mean rotor speed of 275 rpm. It can be seen from the graphical results that the output voltage (Fig. 11 (a)) and the rotational speed (Fig. 11 (d)) are less variable in the APC algorithm than in the case of the PID controller. The mean power captured with the APC control strategy is slightly higher than the power captured with the PID controller (Fig. 11 (c)). The power fluctuation is also less variable with the APC controller, which in addition to the stress (see below) reduction represents the main contribution of the proposed approach. In order to further quantify the results a comparison of the tracking performance of the APC and the PID controllers is performed by using an evaluation index presented in Minchala-Avila et al. (2016), which is defined as follows:

$$E = \sum_{k=0}^{\infty} |e(k)|^2 + \sum_{k=0}^{\infty} |u(k)|^2 \tag{8}$$

where,

$e(k) = v_{ref}(k) - v_{out}(k)$ → Voltage tracking error

$u(k)$ → Control signal

Fig. 11 (f) shows the instantaneous response of this index (which can be interpreted as the control effort), that shows a more consistent behavior for the APC controller.

Fig. 12 shows another comparison between the performance of the APC and the reference PID controller, where Fig. 12 (a) has the output power time series and Fig. 12 (b) the stress time series. It can be seen that the output power time series are quite similar in both cases,

whereas the stress time series show significant differences. Though the average stress is very similar in both control schemes the fluctuating component is much higher in the case of the PID control. This is further illustrated by the normalized spectral density of both power and stress (Figures 12 (c) and 12 (d)), showing a dramatic reduction in the stress amplitude spectrum, as well as a mild reduction in power fluctuations. This significant reduction in the fluctuating components of the blade stress has a direct impact on the reduction of fatigue stress and hence fatigue degradation of the blade. From the comparison in Fig. 12 (d) it is clear the APC allows for a dramatic reduction of all spectral stress components compared to the reference PID case, with a typical reduction by a factor of 2 at most spectral peaks. Table 2 shows a summary of the results just presented. The reduction in stress variability also leads to smaller extreme values, as illustrated by the fact that the normalized stress never overpasses the maximum value of the material strength, which corresponds to $\xi = 1$. In contrast, the WECS operation with the PID controller presents two events where $\xi > 1$, potentially compromising the structural integrity of the blades.

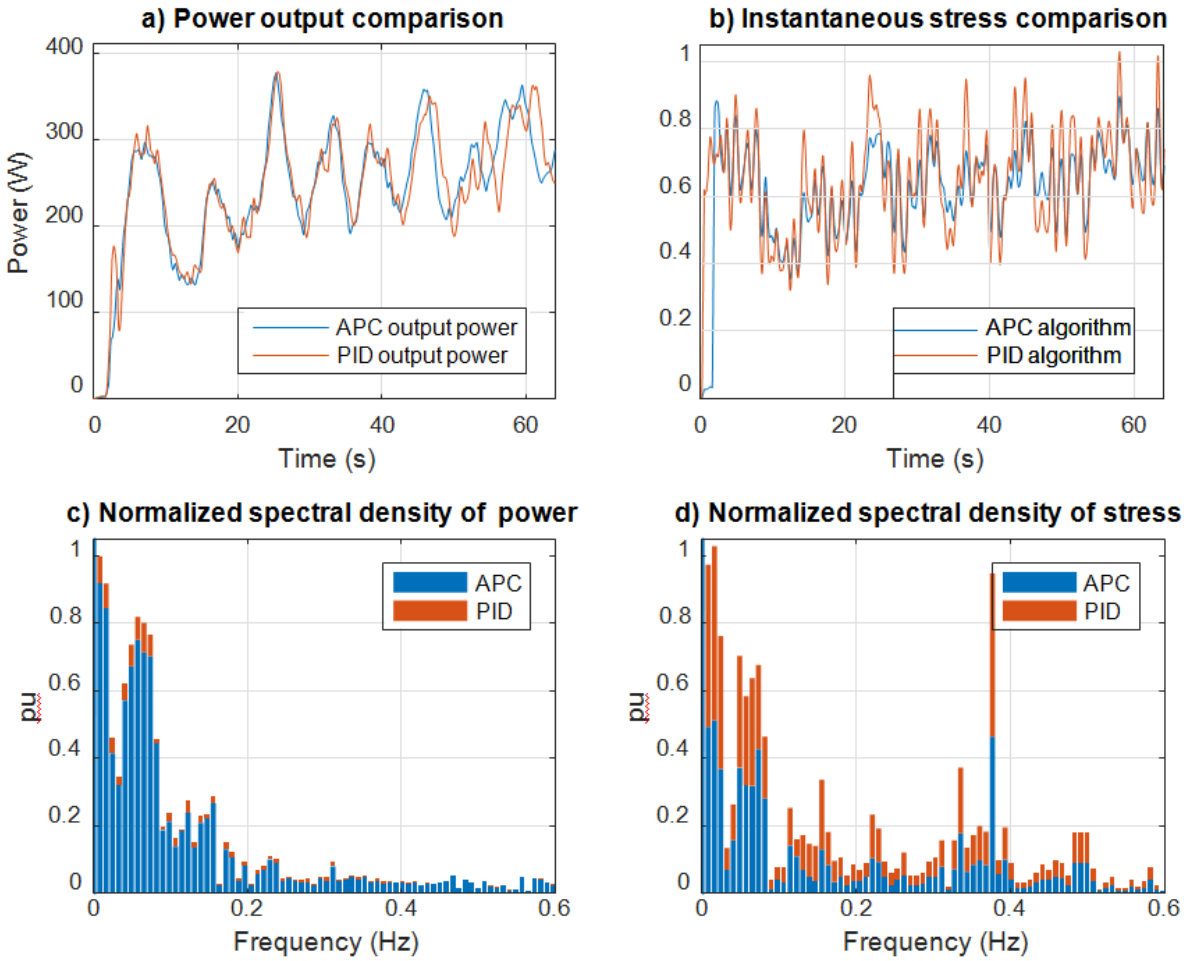

Fig. 12. Controllers' transient and frequency responses performance comparison.

Table 2. Summary of the controllers' performance comparison shown in Fig. 12.

	PID Algorithm	APC algorithm
$mean(\xi)$	0.644	0.587
$\max(\xi_{fft})$	1	0.502
$mean(P)$	243.8 W	242.4 W
$\max(P_{fft})$	1	0.942
$\sum \xi_i > 1$	2	0

The accuracy of the control achieved with both strategies (APC and PID) is illustrated in Fig. 13, where the phase portraits of the system trajectories in the stress-power plane are shown; for both variables the difference between the actual and the set-point value are shown. The APC phase portrait (Fig. 13 (a)) can be seen to be much more compact, with a smaller overall size and a far smaller number of outliers compared to the reference PID control (Fig. 13 (b)), evidencing a generally better control performance.

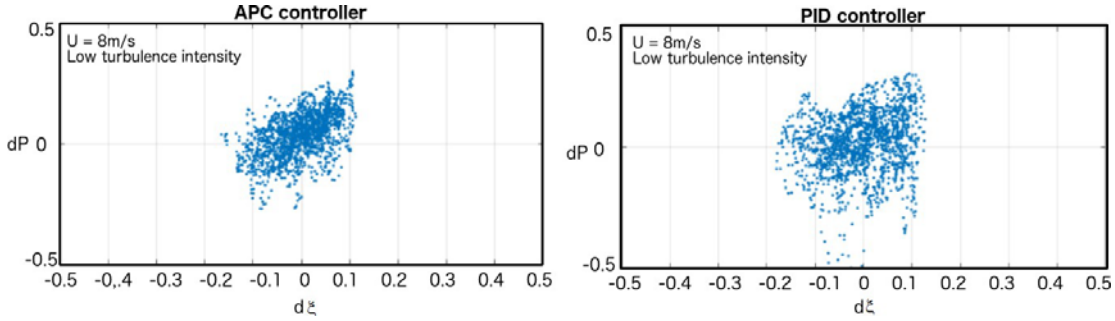

Fig. 13. Phase portrait of the system trajectories around the optimal set-point.

The experimental results show that (1) the APC approach allows for a more accurate control compared to the reference PID scheme, (2) the improved control directly translates into a lower level of stress fluctuations at the blades, leading to reduced fatigue and extreme stress, (3) the use of a compound power-stress cost function allows for a conceptually simple away of conducting a bi-objective control, and (4) the penalty incurred in terms of power reductions upon reducing blades stresses is low, leading to a very favorable trade-off. As an added value, the method proposed allows for a technological upgrade of an existing SWT in order to achieve an enhanced operation, which ensures a longer life cycle. The upgrade consists of installing a customized controlled rectifier in the conversion system, in replacement of the non-controlled rectifier and implementing the simple APC scheme outlined in the present work, leaving all other system components unchanged, in particular the grid-controlled inverter. This plug-in upgrade will boost the lifetime of the mechanical components of the system through a reduced fatigue stress spectrum and lower extreme stresses, while reducing the power/energy output only by a small fraction. While the cost function presented in the current work considers only rotor blade stresses, a generalization to other mechanical components is straightforward, including the possibly of conducting a higher-order multi-objective control by considering additional stress functions.

5. CONCLUSIONS

In the present work, a novel control scheme for small wind turbines based on a two-layer scheme using an adaptive predictive control (APC) has been designed, implemented on a test rig emulating the dynamic behavior of a 3kW fixed-pitch wind turbine, and shown to have superior regulation capabilities compared to a reference PID system. Additionally, a compound cost function, combining the normalized power output and the normalized blade stress function, was constructed and used for controlling the small wind turbine operation. Experimental evidence, rep- resented in different formats, clearly demonstrates that the novel scheme achieves a significant reduction (typically of the order of 0.1 p.u.) of the median stress for a given output power level or, conversely, an increase in output power for a given stress level. Apart from this favorable trade-off between average stress and average power the new method is shown to reduce fatigue stress amplitudes at all frequencies, as well as extreme stresses, thereby boosting the wind turbines life time and reliability. An added benefit of the innovation is the fact that an existing small wind turbine system can be easily upgraded by replacing the common fixed rectifier by a controlled one and adding a small box with the switching electronics and control algorithm, conveniently implemented in two small microcontrollers. No other changes are necessary in the system, given the two-layer architecture of the control scheme proposed. The expected benefit, so far demonstrated on the laboratory level, is a longer life time of the mechanical components at a small energy penalty. While the current scheme uses a static cost function, obtained from an off-line calculation, future versions of the present scheme might be able to incorporate on-line measurements of blade stresses and accelerations to continuously update the cost function and account for changing conditions and aging.

ACKNOWLEDGEMENTS

Support of this project by the Mexican Center for Innovation in Wind Energy (CEMIE Eólico) under project number P19 is gratefully acknowledged.

REFERENCES

Bobrow, J.E. and Murray, W. (1993). An algorithm for rls identification parameters that vary quickly with time. *IEEE Transactions on Automatic Control*, 38(2), 351–354. doi:10.1109/9.250491.

Bottasso, C.L., Croce, A., Riboldi, C.E., and Salvetti, M. (2014). Cyclic pitch control for the reduction of ultimate loads on wind turbines. In *Journal of Physics: Conference Series*, volume 524. doi:10.1088/1742- 6596/524/1/012063.

Cárdenas, D., Probst, O., and Elizalde, H. (2018). Progressive failure analysis of wind turbine blades under stochastic fatigue loads. *Ingeniería Mecánica, Tecnología y Desarrollo*, 5(6), 15.

Chidrawar, S. and Patre, B. (2008). Generalized Predictive Control and Neural Generalized Predictive Control. *Leonardo Journal of Sciences*, 7(13), 133–152.

Clarke, D., Mohtadi, C., and Tuffs, P. (1987). Generalized predictive control Part I. The basic algorithm. *Automatica*, 23(2), 137–148. doi:10.1016/0005-1098(87)90087-2.

Elizondo, J., Martínez, J., and Probst, O. (2009). Experimental study of a small wind turbine for low- and medium-wind regimes. *International Journal of*

Energy Research, 33(3), 309–326. doi:10.1002/er.1482.URL http://doi.wiley.com/10.1002/er.1482.

Frost and Sullivan (2017). Global Wind Power Market, Forecast to 2025.

Ghosh, S.K., Shawon, M.H., Rahman, M.A., and Nath, S.K. (2014). Wind energy assessment using Weibull Distribution in coastal areas of Bangladesh. In 2014 *3rd International Conference on the Developments in Renewable Energy Technology (ICDRET)*, 1–6. doi: 10.1109/ICDRET.2014.6861731.

González, L.G., Figueres, E., Garcerá, G., and Carranza, O. (2010). Maximum-power-point tracking with reduced mechanical stress applied to wind-energy-conversion- systems. *Applied Energy*, 87(7), 2304–2312. doi: 10.1016/j.apenergy.2009.11.030.

Gupta, A. and McIntyre, A. (2017). Hype Cycle for Sustainability Technology. Technical report, Gartner.

Habibi, H., Koma, A., and Howard, I. (2017). Power improvement of non-linear wind turbines during partial load operation using fuzzy inference control. *Control Engineering and Applied Informatics*, 19(2), 31–42.

Han, Y. and Leithead, W.E. (2014). Combined wind turbine fatigue and ultimate load reduction by individual blade control. In *Journal of Physics: Conference Series*, volume 524. doi:10.1088/1742-6596/524/1/012062.

Han, Y. and Liu, X. (2014). Collective pitch sliding mode control for large scale wind turbines considering load reduction. In *Mechatronics and Control (ICMC), 2014 International Conference on*, 652–656. doi:10.1109/ICMC.2014.7231635.

Iordanov, S.G., Collu, M., and Cao, Y. (2017). Can a Wind Turbine Learn to Operate Itself? Evaluation of the potential of a heuristic, data-driven self-optimizing control system for a 5MW offshore wind turbine. In Energy Procedia, volume 137, 26–37. doi: 10.1016/j.egypro.2017.10.332.

Meng, F., Wenske, J., and Gambier, A. (2016). Wind turbine loads reduction using feedforward feedback collective pitch control based on the estimated effective wind speed. In Proceedings of the American Control Conference, volume 2016-July, 2289–2294. doi: 10.1109/ACC.2016.7525259.

Minchala, L.I., Probst, O., and Cardenas-Fuentes, D. (2018). Wind turbine predictive control focused on the alleviation of mechanical stress over the blades. IFAC-PapersOnLine, 51(13), 149-154.

Minchala, L.I., Cardenas-Fuentes, D., and Probst, O. (2017). Control of mechanical loads in wind turbines using an integrated aeroelastic model. In 2017 IEEE PES Innovative Smart Grid Technologies Conference - Latin America (ISGT Latin America), 1–6. IEEE. doi: 10.1109/ISGT-LA.2017.8126732.

Minchala-Avila, L.I., Palacio-Baus, K., Ortiz, J.P., Valladolid, J.D., and Ortega, J. (2016). Comparison of the performance and energy consumption index of model-based controllers. In 2016 IEEE Ecuador Technical Chapters Meeting (ETCM), 1–6. doi: 10.1109/ETCM.2016.7750825.

Mishnaevsky, L., Brøndsted, P., Nijssen, R., Lekou, D.J., and Philippidis, T.P. (2012). Materials of large wind turbine blades: recent results in testing and modeling. Wind Energy, 15(1), 83–97. doi:10.1002/we.470.

Petrovic, V., Jelavic, M., and Baotic, M. (2015). Advanced control algorithms for reduction of wind turbine structural loads. Renewable Energy, 76, 418–431. doi: 10.1016/j.renene.2014.11.051.

Scarlat, A., Munteanu, I., and Bratcu, A. (2012). Control law design of a low-power wind energy system using active speed stall techniques. Control Engineering and Applied Informatics, 14(3), 15–24.

Selvam, K., Kanev, S., Van Wingerden, J.W., Van Engelen, T., and Verhaegen, M. (2009). Feedback feedforward individual pitch control for wind turbine load reduction. International Journal of Robust and Nonlinear Control, 19(1), 72–91. doi:10.1002/rnc.1324.

Senanayaka, J.S.L., Karimi, H.R., and Robbersmyr, K.G. (2017). A novel soft-stall power control for a small wind turbine. In 2017 IEEE 26th International Symposium on Industrial Electronics (ISIE), 940–945. IEEE. doi: 10.1109/ISIE.2017.8001372.

UNFCCC (2015). Paris Agreement doi:FCCC/CP/2015/L.9/Rev.1 URL https://goo.gl/BJJkKA.

Wymore, M.L., Van Dam, J.E., Ceylan, H., and Qiao, D. (2015). A survey of health monitoring systems for wind turbines. Renewable and Sustainable Energy Reviews, 52, 976–990. doi: 10.1016/j.rser.2015.07.110.

Yang, W., Tavner, P.J., Crabtree, C.J., Feng, Y., and Qiu, Y. (2014). Wind turbine condition monitoring: Technical and commercial challenges. Wind Energy, 17(5), 673–693. doi:10.1002/we.1508.